IEEE Access
Multidisciplinary | Rapid Review | Open Access Journal

Received February 23, 2019, accepted March 17, 2019, date of publication March 26, 2019, date of current version April 15, 2019.

Digital Object Identifier 10.1109/ACCESS.2019.2907288

Inversion of Oil-Immersed Paper Resistivity in Transformer Based on Dielectric Loss Factor

JIANGJUN RUAN[1], (Member, IEEE), YIMING XIE[1], (Member, IEEE), SHUO JIN[2], YU SHI[3], YU TIAN[1], AND YONGQING DENG[1]

[1]School of Electrical Engineering and Automation, Wuhan University, Wuhan 430072, China
[2]School of Electrical and Electronic Engineering, Hubei University of Technology, Wuhan 430068, China
[3]School of Electrical and Information Engineering, Anhui University of Science and Technology, Huainan 232001, China

Corresponding author: Yiming Xie (xieyiming@whu.edu.cn)

This work was supported in part by the School of Electrical Engineering and Automation, Wuhan University.

ABSTRACT The aging of the transformer oil–paper insulation distributes spatially, which results in changes in paper resistivity in different regions. This paper establishes an iterative inversion algorithm using the finite element method to calculate the oil-immersed paper resistivity in different regions of a transformer. This algorithm sets the transformer dielectric loss factor tan δ at low frequency, the dielectric parameters of the transformer oil as inputs and the oil-immersed paper resistivity as output. The resistivity obtained from inversion can be used as a reference to access the insulation state of the oil–paper insulation. This paper aims at achieving the nondestructive detection of the partial state of the oil–paper insulation.

INDEX TERMS Inversion, oil-immersed paper resistivity, dielectric loss factor, Newton-Raphson method, transformer.

I. INTRODUCTION

Oil immersed power transformers are widely used in power supply and distribution systems. At present, insulation failure is the main cause of transformer failure [1]. The internal insulation of an oil-immersed transformer is comprised of an oil-paper insulation system. Because the oil sample is easy to obtain during operation, the ageing state of the oil can be conveniently detected and ageing oil can be replaced by new oil [2]–[4]. However, due to the electric field and thermal effects, the ageing state of oil-immersed paper or paperboard is uneven. In addition, it is difficult to extract oil-immersed paper sample nondestructively from a transformer [5], [6]. The insulative and mechanical properties would be damaged irreversibly once deterioration occurred. Hence, the ageing degree of the oil-immersed paper determines the insulation state of transformer [7]–[9].

To address the condition monitoring of transformer oil-paper insulation, the present assessment methods include analysis of furaldehyde, the dissolved gas analysis (DGA), the recovery voltage method (RVM), polarization and depolarization current (PDC) and frequency dielectric spectroscopy (FDS). The degree of polymerization (*DP*) is an important basis for assessing the ageing condition of paperboard. Many studies have shown that *DP* had a significant relationship with furaldehyde and other dissolved gases in oil [10]–[12]. DGA is a widely used online monitoring method. However, the analysis of furaldehyde and DGA are both influenced by the replacement of oil [4], [13], [14]. RVM, PDC and FDS are dielectric response method. The first two are implemented in the time domain, and FDS is implemented in the frequency domain. Nevertheless, these methods cannot assess the local ageing in oil-paper insulation caused by uneven electrothermal effects [15]–[17], and the results may be affected by the oil.

In conclusion, current condition assessment methods for oil-paper insulation fail to distinguish the insulation condition at various regions in transformer internal insulation. To solve this problem, a new approach, the iterative inversion method for oil-immersed paper resistivity, is put forward in [27]. Reference [27] explores the method of resistivity inversion and uses finite element electrostatic field simulation to realize the inversion of resistivity based on the steady-state insulation resistance. To ascertain more input, this paper explores the feasibility of tanδ as an inversion input. Then, this paper takes the tanδ at low frequency and the dielectric parameters of oil as inputs to calculate the oil-immersed paper resistivity in various regions of the transformer based on finite element time harmonic field simulations. Meanwhile, the influence of the initial value on the inversion algorithm is discussed.

The associate editor coordinating the review of this manuscript and approving it for publication was Mehdi Bagheri.

II. INVERSION CONCEPT

Some parameters that characterize the physical model may not be obtained directly from the external measurements. To obtain the information of these parameters, it is necessary to infer these through some measured values, which are related to the parameters. This process is known as inversion, which infers the internal parameters of the model according to the external observed data [18]. For example, resistivity inversion has been widely used in geophysical exploration, especially in mineral and hydrogeological exploration [19], [20].

Because transformers are sealed, it is very difficult to obtain the ageing state of oil-immersed paper directly. Therefore, the resistivity inversion method is applicable to this problem. This method use external measurable parameters to infer the material parameters of internal oil-immersed paper and use this parameter as a reference for the internal insulation state. The mapping relationship between external measurability (tanδ at low frequency) and the internal ageing characteristics of the transformer (oil-immersed paper resistivity) is established by finite element simulation as follows.

$$F(\boldsymbol{x}) = \boldsymbol{y} \tag{1}$$

where $\boldsymbol{x}$ is the internal ageing transformer characteristic, and $\boldsymbol{y}$ is the external measurability. F is the mapping relationship obtained by finite element simulation. Based on these mapping relationships, values for $\boldsymbol{x}$ are calculated inversely.

A. OUTPUT OF INVERSION

The ageing of oil-immersed paper will cause a change in dielectric parameters. During the ageing process of oil-immersed paper, the interaction between the molecules is weakened gradually, accompanied by the production of polar substances, which cause a decrease in oil-immersed paper resistivity. Reference [21] showed that the conductivity of oil-paper increases with the increased ageing. This is because cellulose pyrolysis produces ageing by-products, such as carboxylic acid, which results in an increase in the number of carriers and a decrease in resistivity. Reference [15] drew similar conclusions. High conductivity will increase local dielectric loss, cause overheating and accelerate ageing [22]. Therefore, resistivity is one of the indexes reflecting the insulation state of oil-immersed paper. Meanwhile, *DP* is generally accepted as an effective basis for evaluating the ageing state of oil-immersed paper, which can effectively reflect the insulation state of oil-immersed paper [23]–[25]. Some researchers have established the relationship between *DP* and the resistivity of oil-immersed paper in [26] by experiments, as shown in Fig. 1. The oil of No. 25 and No. 45 represents different kinds of oil. The relation between the *DP* and the resistivity is derived as (2). Due to (2), the oil-immersed paper resistivity is closely related to *DP*.

$$\rho = A \times DP^K \tag{2}$$

where A and K are constants, and ρ is the resistivity of oil-immersed paper in Ω·m.

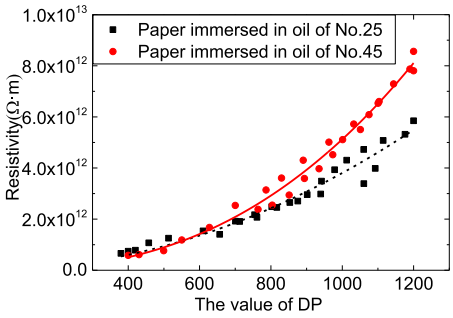

FIGURE 1. Relationship between DP and oil-immersed paper resistivity in [26].

B. INPUT OF INVERSION

In [27], steady-state insulation resistance was used as inversion input. However, the input is too singular, which is not conducive to the division of ageing regions. To solve this problem, this paper explores new inputs. The following content analyses the feasibility of using low-frequency dielectric loss factor as input. Under alternating current (AC) voltage, $U(t) = U_{\mathrm{m}}\sin\omega t$, where U_{m} is the voltage amplitude in V, and ω is the angular frequency in rad/s, According to [28], the definition of dielectric loss factor tanδ of a single dielectric is,

$$\tan\delta = \frac{\varepsilon''}{\varepsilon'} = \frac{1/(\omega\varepsilon_0\rho) + \chi''(\omega)}{1 + \chi'(\omega)} \tag{3}$$

where ε' and ε'' are the real and imaginary part of the complex permittivity, ε_0 is the vacuum permittivity of 8.85×10^{-12} F/m, $\chi'(\omega)$ and $\chi''(\omega)$ are the real and imaginary part of the complex electric susceptibility, $\chi''(\omega)$ is related with the dipole polarization loss, and ρ is the dielectric resistivity in Ω·m.

$$\begin{aligned}\chi''(\omega) &= (\varepsilon_s - \varepsilon_\infty)\frac{\omega\tau}{1+(\omega\tau)^2}\\ \chi'(\omega) &= \varepsilon_\infty - 1 + (\varepsilon_s - \varepsilon_\infty)/[1+(\omega\tau)^2]\end{aligned} \tag{4}$$

where ε_{s} is the dielectric relative permittivity, ε_∞ is the dielectric high-frequency relative permittivity, τ is the time constant of polarization in s.

According to (3) and (4), tanδ has a great relationship with the dipole polarization phenomenon. The loss produced by dipole polarization varies with frequency, whose process is difficult to characterize in the finite element electric field simulation. Therefore, it is necessary to select the frequency section of FDS that can neglect the impact of dipole polarization loss on tanδ.

When applied the voltage is at low frequency, ω is close to 0, and the tanδ can be rewritten as follows.

$$\tan\delta = 1/\omega\varepsilon_0\varepsilon_s\rho \tag{5}$$

At low frequency of voltage, the electric field changes slowly. Because the built-up time of dipole polarization is approximately $10^{-6} \sim 10^{-2}$ s, the dipole polarization has enough time to establish. The period of dipole rotation does not lag behind the period of electric field change. Therefore, the energy produced by the dipole polarization can be

neglected, namely, $\chi''(\omega) \approx 0$. The loss of conductance is the main loss [17]. In summary, the tanδ is closely related to its resistivity at low frequencies.

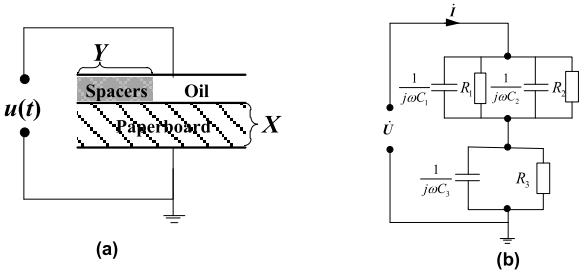

FIGURE 2. Equivalent model of oil-paper insulation. (a) XY model. (b) Equivalent circuit.

The oil-paper insulation system, as a compound material, can be equivalent to an XY model [29]. The equivalent model is shown in Figure 2. Spacers, oil, and paperboard resistivity and relative permittivity are ρ_1, ε_1,ρ_2, ε_2 and ρ_3, ε_3 respectively, Spacers, oil, and paperboard resistance and capacitance are R_1, C_1, R_2, C_2 and R_3, C_3 respectively, X is the ratio of paperboard thickness to the total thickness of the main insulation between high- and low-voltage windings. Y is the ratio of the spacer width to the average circumference of the main insulation between the high- and low-voltage windings. Generally, $X \in [0.2, 0.5]$, $Y \in [0.15, 0.25]$ [29]. The total tanδ can be derived in Figure 2 as:

$$\tan\delta_{mix} = (C_1 \tan\delta_1 + C_2 \tan\delta_2)/(C_1 + C_2) \tag{6}$$

$$\tan\delta = \frac{C_3 \tan\delta_{mix}(1+\tan^2\delta_3)+(C_1+C_2)\tan\delta_3(1+\tan^2\delta_{mix})}{(C_1+C_2)(1+\tan^2\delta_{mix})+C_3(1+\tan^2\delta_3)} \tag{7}$$

where tanδ_1, tanδ_2 and tanδ_3 is the dielectric loss factors of spacers, oil, and paperboard, respectively; tanδ_{mix} is the total dielectric loss factor of spacers and oil.

In (7), only tanδ_1, tanδ_2 and tanδ_3 are related to ω; other items do not contain ω. According to (5), the tanδ of the XY model can also neglect the effect of dipole polarization loss in each single dielectric at low frequency.

$$\begin{cases} \tan\delta_1 = 1/\omega\varepsilon_0\varepsilon_1\rho_1 \\ \tan\delta_2 = 1/\omega\varepsilon_0\varepsilon_2\rho_2 \\ \tan\delta_3 = 1/\omega\varepsilon_0\varepsilon_3\rho_3 \end{cases} \tag{8}$$

$$\begin{cases} C_1 = \varepsilon_0\varepsilon_1 YA/(1-X) \\ C_2 = \varepsilon_0\varepsilon_2(1-Y)A/(1-X) \\ C_3 = \varepsilon_0\varepsilon_2 A/X \end{cases} \tag{9}$$

where A is the width of the medium.

The dielectric response of the XY model affected by the paper dielectric parameter (ρ and ε) at low frequency

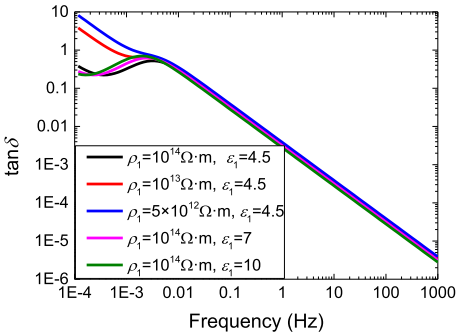

FIGURE 3. FDS under different paper dielectric parameters.

is discussed as follows. In the ageing process, the ρ of paper decreases with ageing, while the ε increases with ageing [26], [30]. Generally, the resistivity of paperboard and transformer oil ranges on the order of $10^{14}\Omega$·m and $10^{12}\Omega$·m, respectively. Considering the influence of change range in paper resistivity and the relative permittivity on the FDS, the FDS of different paper dielectric parameters is calculated through (7), (8), and (9) as shown in Fig. 3, where $X = 0.5$, $Y = 0.2$, $\rho_1 = 1 \times 10^{12}$ Ω·m, $\varepsilon_2 = 2.2$, and $\varepsilon_0 = 8.85\times10^{-12}$ F/m. Because the spacers and paperboard are the same material, so $\rho_1 = \rho_3$, $\varepsilon_1 = \varepsilon_3$. According to [26] and [30], the ρ_1 ranges from 1×10^{14} Ω·m to 5×10^{12} Ω·m, and ε_1 ranges from 4.5 to 10.

As shown in Fig. 3, when the ρ of paper decreases from 1×10^{14} Ω·m to 5×10^{12} Ω·m, the low-frequency curve moves upward, whereas the low-frequency section of the curve did not change remarkably when the $\varepsilon$of paper increases from 4.5 to 10.

When the external voltage excitation is at low frequency, the electric field distribution is proportional to the resistivity. The relative permittivity of the paper is approximately 2 times than that of the transformer oil, while its resistivity is $10^1 \sim 10^2$ times than that of the transformer oil. Overall, in the low-frequency electric field, the oil-immersed paper undertakes the main voltage drop, so the low-frequency section of FDS mainly reflects the change of oil-immersed paper resistivity. The above conclusion is similar to the experimental results in [31]. In [31], the influence of different water content on the FDS of oil-immersed paper was studied under the same ageing state. The increase of moisture content will lead to the decrease of resistivity, which indirectly shows that tanδ at the low frequency mainly embodies the change of oil-immersed paper resistivity.

In short, the tanδ values at the low frequency of the oil-paper insulation are influenced greatly by the change of the oil-immersed paper resistivity; meanwhile, the dipole polarization loss of each layer has little influence on the tanδ at low frequency. Therefore, the low-frequency tanδ can be used as the inversion input to calculate the oil-immersed paper resistivity. The inversion frequency is set to 10^{-3} Hz in this paper.

III. INVERSION ALGORITHM

A. INVERSION MODEL

According to the analysis of Section II, when the applied voltage is at low frequency, a mapping relationship F is established through finite element time harmonic field simulation as follows.

$$F(\rho, \varepsilon, \rho_{oil}, \varepsilon_{oil}) = \tan\delta \tag{10}$$

where ρ and ε are the average resistivity and relative permittivity of oil-immersed paper. ρ_{oil} and ε_{oil} are the average resistivity and relative permittivity of the transformer oil. The ρ_{oil} and ε_{oil} can be measured through sampling, which are set as known. According to Figure 3, the change of relative permittivity of oil-immersed paper has little impact on tanδ at low frequency compared with resistivity. Therefore, this paper neglects the effect of ε, which is set as 4.5 in this paper. Equation (10) is written into (11).

$$F(\rho) = \tan\delta \tag{11}$$

Because of the complexity of the insulation structure in transformer, F cannot be obtained from analytic formula. To obtain the relationship F in (11), this paper built a two-dimensional (2D) finite element axisymmetric model as shown in Fig. 4.

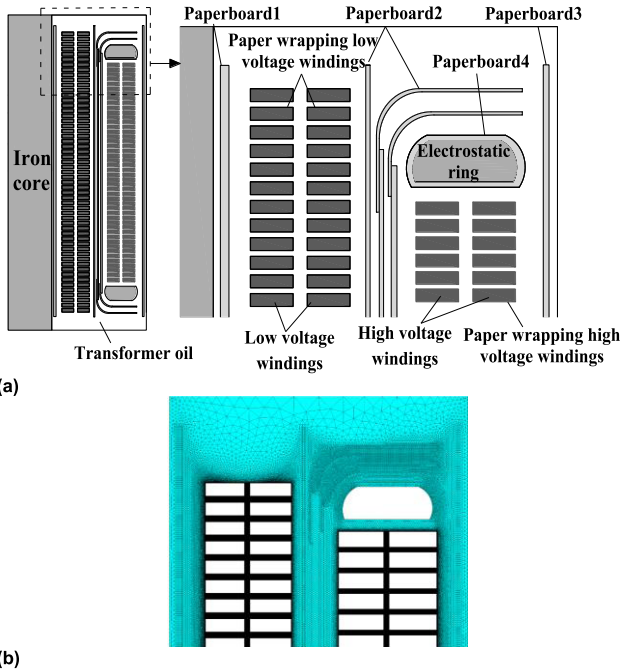

FIGURE 4. (a) 2-D axisymmetric finite element model and (b) local mesh grid of transformer.

In Fig. 4(a), the oil-immersed paper is wrapped outside the high- and low-voltage winding, and the insulation paperboards are set between the high- and low-voltage winding, the low-voltage winding and the iron core, and the high-voltage winding and the transformer shell. They are all immersed in transformer oil. Because the spacers are parallel with the oil duct, and the resistance of the oil is much lower than that of the spacers. Therefore, this paper neglected the spacer effect.

In the process of finite element time harmonic field simulation, Solid 231 element is used, and triangular mesh is selected for meshing. The mesh grid is shown in Fig. 4(b).

B. NEWTON-RAPHSON METHOD

An iterative method can solve nonlinear equations [27], [32] with fast convergence speed and is suitable for high-dimensional complex computations. The Newton-Raphson method is the most widely used iterative method, which adopts a linear equation instead of nonlinear equations to establish an iterative format. Therefore, the Newton-Raphson method is used to solve the oil-immersed paper resistivity ρ in (11) inversely.

1) MULTI-REGIONAL RESISTIVITY INVERSION METHOD

In practical engineering, the deterioration of the oil-paper insulation occurs in the local areas due to electro-thermal ageing. Therefore, to consider the spatial dispersion of insulation ageing and roughly distinguish the weak areas of ageing, it is necessary to obtain the paper or paperboard resistivity in different regions.

The mathematical model for inversion of resistivity in different regions is to solve nonlinear equations. Multiple-solutions are the main problem conducting inversion [18]. In order to guarantee the uniqueness of the solution, it is necessary to guarantee the positive definiteness of equations and the independence between the equations. Hence, different voltage loadings are used to increase the mapping relationships. The oil-immersed paper inside the transformer is divided into N regions. The equations can be expressed as (12).

$$\begin{cases} F_1(\rho_1, \rho_2, \ldots \rho_N) = \tan\delta_1 \\ F_2(\rho_1, \rho_2, \ldots \rho_N) = \tan\delta_2 \\ \vdots \\ F_N(\rho_1, \rho_2, \ldots \rho_N) = \tan\delta_N \end{cases} \tag{12}$$

where the mapping relationships $F_1, F_2, \ldots F_N$ indicate the mapping relationships caused by different voltage loadings, and $\rho_1, \rho_2, \ldots \rho_N$ represent oil-immersed paper in$N$ different regions. tanδ_1, tanδ_2, …tanδ_N represent the corresponding port dielectric loss factor under N voltage loadings.

The Newton-Raphson method is used to solve the nonlinear equations as follows:.

(1) Set the initial resistivity value in N regions as $\rho_{10}, \rho_{20}, \cdots \rho_{N0}$;

(2) Calculate the tanδs under different voltage loadings corresponding to the initial resistivity through the finite element time harmonic field simulation, that is, tan$\delta_{10}(\rho_{10}, \rho_{20}, \ldots \rho_{N0})$, tan$\delta_{20}$ $(\rho_{10}, \rho_{20}, \ldots \rho_{N0})$,…tan$\delta_{N0}$ $(\rho_{10}, \rho_{20}, \ldots \rho_{N0})$;

(3) Identify the errors $\sigma_1, \sigma_2, \cdots \sigma_N$ between the measured value $\tan\delta_{1r}, \tan\delta_{2r}, \ldots \tan\delta_{Nr}$ and the $\tan\delta$s in step (2). If all errors are less than σ_{stop}, the iteration terminates. In addition, the resistivity in various regions in the previous step is the actual resistivity. Otherwise, step (4) is executed.

(4) Calculate the partial derivatives of $\tan\delta_{10}$, $\tan\delta_{20}$, $\cdots \tan\delta_{N0}$ to ρ_1, $\rho_2, \cdots \rho_N$ to form a Jacoby matrix. The formula of the partial derivative of $\tan\delta_{10}$ to ρ_1 is taken as an example in (13).

$$\frac{\partial \tan\delta_{10}}{\partial \rho_1} = \frac{\tan\delta_{10}(\rho_1 + \delta\rho_1, \rho_2, \ldots \rho_N) - \tan\delta_{10}(\rho_1, \rho_2, \ldots \rho_N)}{\delta\rho_1} \tag{13}$$

where $\delta\rho$ is a small positive.

The Jacoby matrix J is in (14), as shown at the bottom of this page.

(5) Equation (15) is used to calculate the corrections of ρ_1, $\rho_2, \cdots \rho_N$.

$$\begin{bmatrix} \Delta\rho_1 \\ \Delta\rho_2 \\ \vdots \\ \Delta\rho_N \end{bmatrix} = J^{-1} \begin{bmatrix} \Delta\tan\delta_1 \\ \Delta\tan\delta_2 \\ \vdots \\ \Delta\tan\delta_N \end{bmatrix} \tag{15}$$

where $\Delta tan\delta_1 = tan\delta_{1r} - tan\delta_{10}(\rho_{10}, \rho_{20}, \cdots, \rho_{N0})$, $\Delta tan\delta_2 = tan\delta_{2r} - tan\delta_{20}(\rho_{10}, \rho_{20}, \cdots, \rho_{N0}), \cdots \Delta tan\delta_N = tan\delta_{Nr} - tan\delta_{N0}(\rho_{10}, \rho_{20}, \cdots, \rho_{N0})$;

(6) The $\rho_1, \rho_2, \cdots \rho_N$ are corrected according to the corrections in (15):

$$\begin{aligned} \rho_{11} &= \rho_{10} + \Delta\rho_1, \\ \rho_{21} &= \rho_{20} + \Delta\rho_2, \\ &\cdots \\ \rho_{N1} &= \rho_{N0} + \Delta\rho_N \end{aligned}$$

where $\rho_{11}, \rho_{21}, \cdots \rho_{N1}$ are the first revised values of ρ_1, $\rho_2, \cdots \rho_N$.

(7) Return to step (2) and calculate $\tan\delta_{11}(\rho_{11}, \rho_{21}, \ldots \rho_{N1})$, $\tan\delta_{21}(\rho_{10}, \rho_{21}, \ldots \rho_{N1}), \ldots \tan\delta_{N1}(\rho_{11}, \rho_{21}, \ldots \rho_{N1})$. Repeat step (2) to step (6) until $\sigma_1, \sigma_2, \cdots \sigma_N$ are less than σ_{stop}, and the iteration stops.

The iterative flow chart is as shown in Fig. 5. According to the measurement rules of transformer $\tan\delta$, there are 3 different voltage loadings to measure 3 sets of $\tan\delta$, namely, $N = 3$. The modes of voltage loading are shown in Table 1.

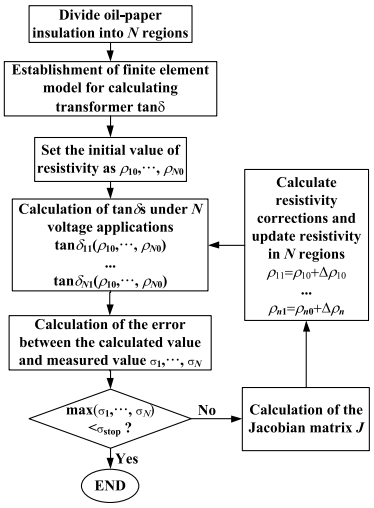

FIGURE 5. Multi-dimensional iterative process.

TABLE 1. Voltage loading modes and corresponding $\tan\delta$.

High voltage	Grounding	$\tan\delta$
High voltage winding	Low voltage winding, iron core and shell	$\tan\delta_{H\text{-}L}$ $\tan\delta_{H\text{-}S}$
Low voltage winding	High voltage winding, iron core and shell	$\tan\delta_{L\text{-}H}$ $\tan\delta_{L\text{-}S}$
High and low voltage winding	Iron core and shell	$\tan\delta_{HL\text{-}S}$

In Table 1, $\tan\delta_{H-L} = tan\delta_{L-H}$, and "H", "L", and "S" represent "high voltage windings", "low voltage windings", and "iron core and shell", respectively.

To calculate $\tan\delta$at low frequency in the finite element time harmonic field simulation, this paper takes the calculation of $\tan\delta_{H-L}$ as an example. First, set the dielectric parameters of the oil and paper, and set frequency $f = 10^{-3}$ Hz. Second, the high voltage $U(\omega)$ and 0 potential are applied on the high and low voltage windings, respectively. The imaginary part and the real part of the current are obtained from the simulation. Finally, the imaginary part divided by the real part is $\tan\delta_{H-L}$.

Therefore, the oil-paper insulation inside the transformer can be divided into 3 regions. Equation (12) can be rewritten as (16)

$$\begin{cases} F_1(\rho_1, \rho_2, \rho_3) = \tan\delta_1 \\ F_2(\rho_1, \rho_2, \rho_3) = \tan\delta_2 \\ F_3(\rho_1, \rho_2, \rho_3) = \tan\delta_3 \end{cases} \tag{16}$$

$$J = \begin{bmatrix} \frac{\partial \tan\delta_{10}(\rho_{10}, \cdots, \rho_{N0})}{\partial\rho_1} & \frac{\partial \tan\delta_{10}(\rho_{10}, \cdots, \rho_{N0})}{\partial\rho_2} & \cdots & \frac{\partial \tan\delta_{10}(\rho_{10}, \cdots, \rho_{N0})}{\partial\rho_N} \\ \frac{\partial \tan\delta_{20}(\rho_{10}, \cdots, \rho_{N0})}{\partial\rho_1} & \frac{\partial \tan\delta_{20}(\rho_{10}, \cdots, \rho_{N0})}{\partial\rho_2} & \cdots & \frac{\partial \tan\delta_{20}(\rho_{10}, \cdots, \rho_{N0})}{\partial\rho_N} \\ \vdots & \vdots & \ddots & \vdots \\ \frac{\partial \tan\delta_{N0}(\rho_{10}, \cdots, \rho_{N0})}{\partial\rho_1} & \frac{\partial \tan\delta_{N0}(\rho_{10}, \cdots, \rho_{N0})}{\partial\rho_2} & \cdots & \frac{\partial \tan\delta_{N0}(\rho_{10}, \cdots, \rho_{N0})}{\partial\rho_N} \end{bmatrix} \tag{14}$$

Because the distribution of the electric field in the transformer is different under 3 voltage loadings, the equations in (16) are independent of each other.

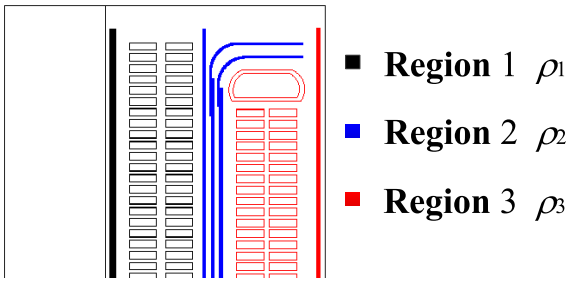

FIGURE 6. Division of insulating paper.

TABLE 2. Actual resistivity.

f/Hz	Initial value of resistivity /Ω·m	Range of resistivity /Ω·m	Oil Resistivity /Ω·m	Oil relative permittivity	Stop error σ_{stop}/%
10^{-3}	0.6×10^{12}	$[0.5\times10^{12}, 1\times10^{18}]$	1×10^{12}	2.2	0.1

To demonstrate the validity of the inversion method, the tanδvalues obtained by the simulation are set to the actual value to analog the tanδ obtained by the test. The oil-paper insulation in Fig. 4 is divided into 3 regions as shown in Fig. 6. This paper sets the actual resistivity of the 3 different regions as $\rho_1 = 1\times10^{13}$, $\rho_2 = 0.5\times10^{13}$, and $\rho_3 = 1\times10^{12}\Omega$·m to represent 3 insulation state types of oil-immersed paper, where ρ_3 indicates ageing in this region. Meanwhile, the $\tan\delta_{H-LS}$, $\tan\delta_{L-HS}$, $\tan\delta_{HL-S}$ under 3 types of voltage loadings corresponding to ρ_1, ρ_2, and ρ_3 are calculated through finite element simulation as 3.9156, 1.5284, and 3.2178, respectively. These 3 tanδ values are input into the inversion algorithm. The other parameter settings of the inversion are shown in Table 2.

The Newton-Raphson method is used for iteration. The iterative data are shown in Table 3, where φ_1, φ_2, and φ_3 are relative errors between the inverse value and the actual value of resistivity. Fig. 7(a) is the iterative process under an initial resistivity value of $0.6\times10^{12}\Omega$·m. Through the inversion calculation with 6 iterative steps, it can be seen that the resistivity of the 3 regions converged to $1\times10^{13}\Omega$·m, $5\times10^{12}\Omega$·m, and $1\times10^{12}\Omega$·m successfully, which shows the validity of the algorithm. To compare the effects of different initial values on the inversion algorithm, the initial resistivity value in the 3 regions is set as $1\times10^{12}\Omega$·m, $5\times10^{12}\Omega$·m, and $1\times10^{16}\Omega$·m. The other parameters remain unchanged, and the iterative results are shown in Fig. 7(b)-(d).

From Fig. 7(a)-(b), it can be seen that the iteration results will not be modified by the upper and lower bounds. By contrast, when the initial value is 5×10^{12} Ω·m, as shown in Fig. 7(c), ρ_3 has been modified once. For $1\times10^{16}\Omega$·m, as shown in Fig. 7(d) $\rho_1$has been modified twice, and ρ_2, ρ_3 have been modified once. It can be predicted that if the resistivity constraints are not set, the iteration results will

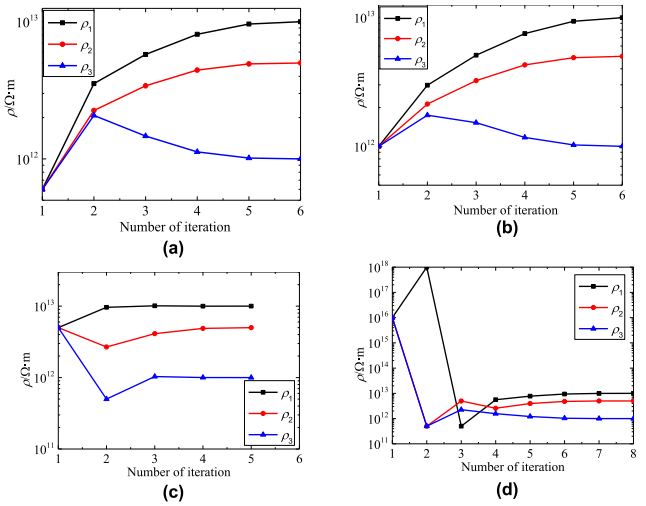

FIGURE 7. The iterative process with different initial resistivity. (a) Initial resistivity of $0.6\times10^{12}\Omega$·m. (b) Initial resistivity of $1\times10^{12}\Omega$·m. (c) Initial resistivity of $5\times10^{12}\Omega$·m. (d) Initial resistivity of $1\times10^{16}\Omega$·m.

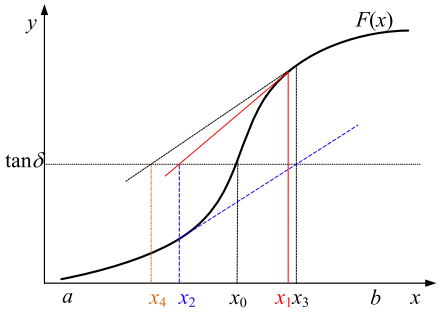

FIGURE 8. Cause analysis of iterative divergence of Newton-Raphson method.

diverge so that the resistivity cannot be inverted. The Newton-Raphson method is sensitive to the selection of initial values, and the results will be divergent because the initial resistivity value is selected improperly. Mathematically, the fundamental reason for this problem is that the second derivative of function $F(x)$ has 0 points in the iteration interval, that is, $\exists x \in [a, b]$, $F''(x) = 0$. In this paper, the one-dimensional nonlinear equation $F(x) = \tan\delta$ is used to explain this problem. Suppose the true root $x = x_0$. The intersection $(x = x_2)$ of the tangent line of curve $F(x)$ at $x = x_1$ and the horizontal line $y = \tan\delta$ is the next value of the iteration. By analogy, the iteration sequence of x, $\{x_1, x_2, x_3, x_4 \ldots\}$ is obtained. From Fig. 8, it can be seen that the direction of concave and convex of curve $F(x)$ has changed in $[a, b]$, namely, the second derivative of $F(x)$ has 0 point, resulting in ''over-correction'' in each iteration; the value obtained is farther and farther from the actual value $x = x_0$, which leads the result to diverge.

In general, to ensure that the roots of nonlinear equations converge effectively, the initial value should be selected near the root. For some practical problems, initial values can

TABLE 3. Simulation iteration process with $\rho_0 = 0.6 \times 10^{12}\Omega$·M.

Iteration number	$\rho_1/\Omega\cdot m\times10^{13}$	$\rho_2/\Omega\cdot m\times10^{13}$	$\rho_3/\Omega\cdot m\times10^{13}$	$\phi_1/\%$	$\phi_2/\%$	$\phi_3/\%$
0	0.06	0.06	0.06	94	88	40
1	0.354	0.225	0.207	64.608	54.949	107.309
2	0.577	0.341	0.147	42.329	31.831	46.733
3	0.809	0.444	0.113	19.094	11.217	12.53
4	0.961	0.493	0.101	3.892	1.495	1.419
5	0.999	0.500	0.10003	0.143	0.0263	0.0303

TABLE 4. Simulation iteration process considering "The Average Effect".

Iteration number	$\rho_1/\Omega\cdot m\times10^{13}$	$\rho_2/\Omega\cdot m\times10^{13}$	$\rho_3/\Omega\cdot m\times10^{13}$	$\phi_1/\%$	$\phi_2/\%$	$\phi_3/\%$
0	0.06	0.06	0.06	94	88	40
1	0.354	0.2253	0.2086	64.605	54.945	108.873
2	0.577	0.3406	0.1487	42.265	31.874	48.667
3	0.811	0.4436	0.1145	18.907	11.274	14.539
4	0.964	0.492	0.104	3.562	1.532	3.492
5	1.002	0.500	0.102	0.250	0.052	2.111

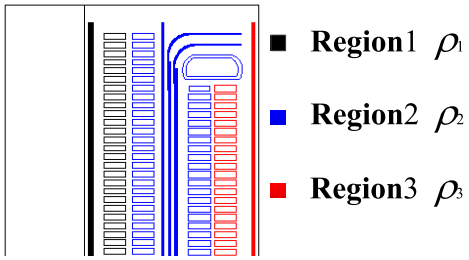

FIGURE 9. Comparison between actual and simulated insulation state partitions.

be selected by experimental and engineering experience to ensure effective convergence.

2) "AVERAGE EFFECT" IN INVERSION

In fact, the ageing locations of oil-paper insulation in a transformer are more random. It is difficult for technicians to obtain the specific ageing parts directly from the outside, so it is difficult to accurately divide the ageing area. Therefore, in this paper, the "average effect" of resistivity is added to the inversion process.

To distinguish the partitions in Fig. 6, paper wrapping the outermost high voltage windings and paperboard (red region) are ageing in Fig. 9, whose resistivity is lower than that of the other regions. The partition in Fig. 9 is thus regarded as the actual insulation partition. However, the inversion simulation is still based on the partition of Fig. 6. The actual value of the resistivity in the 3 regions is still set as $\rho_1 = 1\times10^{13}$, $\rho_2 = 0.5\times10^{13}$, and $\rho_3 = 1\times10^{12}\Omega$·m in order. Meanwhile, the $\tan\delta_{H-LS}$, $\tan\delta_{L-HS}$, and $\tan\delta_{HL-S}$ under 3 types of voltage loadings corresponding to ρ_1, ρ_2, and ρ_3 are calculated through finite element simulation as 3.8981, 1.5240, and 3.2023, respectively, which are regarded as actual values. The initial resistivity value is $0.6\times10^{12}\Omega$·m. The iteration results are shown in Table 4.

It can be seen that ρ_3 in Table 4 is larger than that in Table 3, and φ_3 increases from 0.0303% to 2.111%. This is because region 3 in Fig. 9 is smaller than that of Fig. 6, which makes the inversion calculation synthetically consider the resistivity of region 2 and 3 in Fig. 6, that is, the "average effect". Therefore, the inversed value is the "average" value. In conclusion, the more similar the division in simulation is to the actual division, the closer the resistivity obtained by inversion is to the actual value. In contrast, if the division in simulation is different from the actual division, the "average effect" can reflect the ageing state of a certain region to a certain extent, which also shows that $\tan\delta$ at low frequency can effectively respond to resistivity changes as an inversion input.

IV. CONCLUSION

In this paper, the feasibility of a multi-region inversion method for oil-immersed paper insulation is studied.

(1) The $\tan\delta$ at low frequency and oil resistivity are used as inputs of inversion. Meanwhile, the resistivity of the oil-immersed paper is used as the ageing characteristic, that is, the inversion output.

(2) Through the finite element time harmonic field simulation, the nonlinear mapping relationship between the resistivity of oil-immersed paper and the $\tan\delta$ of the transformer is established. For considering the spatial dispersion of the insulation ageing position in the transformer, the multi-dimensional iteration is realized by the Newton-Raphson method. The simulation results show that the relative errors of resistivity are less than 0.1%, which verifies the correctness of the algorithm. However, if the initial value is not selected properly, it will lead to divergence of inversion results.

(3) Because the technicians may not be able to obtain accurate internal ageing locations directly from the outside of a transformer, this method takes into account the inaccurate division of the ageing region during the inversion process. The results show that the inaccuracy of division in the ageing

region will cause an error in resistivity of the inversion compared with the actual resistivity. However, it can reflect the ageing state of a certain region qualitatively.

In the future, it is necessary to combine the steady-state insulation resistance in [27] and tanδ at low frequency to divide more regions. Meanwhile, the effect of moisture on the resistivity of paperboard should be studied by experiments and using correction coefficients to correct the resistivity of paperboard sample under different moisture content to eliminate the influence of moisture on the resistivity. In the numerical algorithm, further optimization is needed to make the solution converge quickly and accurately. The most important thing is to accurately inverse the ageing state of oil-immersed paper in follow-up experiments, all of which need to be perfected through follow-up studies. The inversion method proposed in this paper provides a new idea in the field of transformer condition assessment.

REFERENCES

[1] W. H. Bartley, "Analysis of transformer failures," in *Proc. 36th Annu. Conf. Int. Assoc. Eng. Insurers*, Stockholm, Sweden, 2003, pp. 1–13.

[2] C. Ekanayake, S. M. Gubanski, A. Graczkowski, and K. Walczak, "Frequency response of oil impregnated pressboard and paper samples for estimating moisture in transformer insulation," *IEEE Trans. Power Del.*, vol. 21, no. 3, pp. 1309–1317, Jul. 2006.

[3] V. G. Arakelian, "Effective diagnostics for oil-filled equipment," *IEEE Elect. Insul. Mag.*, vol. 18, no. 6, pp. 26–38, Nov. 2002.

[4] R. Liao, Y. D. Lin, P. Guo, and H. Liu, "The effects of insulating oil replacement upon power transformer condition assessment," *Electr. Power Compon. Syst.*, vol. 43, no. 17, pp. 1971–1979, 2015.

[5] J. S. N'cho, I. Fofana, Y. Hadjadj, and A. Beroual, "Review of physicochemical-based diagnostic techniques for assessing insulation condition in aged transformers," *Energies*, vol. 9, no. 5, pp. 367–396, 2016.

[6] M. Wang, A. J. Vandermaar, and K. D. Srivastava, "Review of condition assessment of power transformers in service," *IEEE Elect. Insul. Mag.*, vol. 18, no. 6, pp. 12–25, Nov./Dec. 2002.

[7] D. Martin, Y. Cui, C. Ekanayake, H. Ma, and T. Saha, "An updated model to determine the life remaining of transformer insulation," *IEEE Trans. Power Del.*, vol. 30, no. 1, pp. 395–402, Feb. 2015.

[8] M. Arshad and S. M. Islam, "Significance of cellulose power transformer condition assessment," *IEEE Trans. Dielectr. Electr. Insul.*, vol. 18, no. 15, pp. 1591–1598, Oct. 2011.

[9] S. Jin *et al.*, "Charge transport simulation in single-layer oil-paper insulation," *IEEE Trans. Magn.*, vol. 52, no. 3, Mar. 2016, Art. no. 8101404.

[10] A. M. Emsley, X. Xiao, R. J. Heywood, and M. Ali, "Degradation of cellulosic insulation in power transformers. Part 2: Formation of furan products in insulating oil," *IEE Proc.-Sci., Meas. Technol.*, vol. 147, no. 3, pp. 110–114, May 2000.

[11] L. Cheim, D. Platts, T. Prevost, and S. Xu, "Furan analysis for liquid power transformers," *IEEE Elect. Insul. Mag.*, vol. 28, no. 2, pp. 8–21, Mar./Apr. 2012.

[12] H. Malik, Tarkeshwar, and R. K. Jarial, "Make use of DGA to carry out the transformer oil-immersed paper deterioration condition estimation with fuzzy-logic," *Procedia Eng.*, vol. 30, pp. 569–576, 2012. [Online]. Available: https://www.sciencedirect.com/science/article/pii/S1877705812009101

[13] N. Lelekakis, W. Guo, D. Martin, J. Wijaya, and D. Susa, "A field study of aging in paper-oil insulation systems," *IEEE Elect. Insul. Mag.*, vol. 28, no. 1, pp. 12–19, Jan./Feb. 2012.

[14] Y. Lin, L. Yang, R. Liao, W. Sun, and Y. Zhang, "Effect of oil replacement on furfural analysis and aging assessment of power transformers," *IEEE Trans. Dielectr. Electr. Insul.*, vol. 22, no. 5, pp. 2611–2619, Oct. 2015.

[15] T. K. Saha and P. Purkait, "Investigation of polarization and depolarization current measurements for the assessment of oil-paper insulation of aged transformers," *IEEE Trans. Dielectr. Electr. Insul.*, vol. 11, no. 1, pp. 144–154, Feb. 2004.

[16] T. K. Saha and P. Purkait, "Investigation of an expert system for the condition assessment of transformer insulation based on dielectric response measurements," *IEEE Trans. Power Del.*, vol. 19, no. 3, pp. 1127–1134, Jul. 2004.

[17] S. M. Gubanski *et al.*, "Dielectric response methods for diagnostics of power transformers," *IEEE Elect. Insul. Mag.*, vol. 19, no. 3, pp. 12–18, May/Jun. 2003.

[18] M. Sambridge and K. Gallagher, *Encyclopedia of Solid Earth Geophysics*. Dotrich, The Netherlands: Springer, 2011.

[19] G. El-Qady and K. Ushijima, "Inversion of DC resistivity data using neural networks," *Geophys. Prospecting*, vol. 49, no. 4, pp. 417–430, 2010.

[20] Y. Sasaki, "3-D resistivity inversion using the finite element method," *Geophysics*, vol. 59, no. 12, pp. 1839–1848, 2012.

[21] Y. Zhou, M. Huang, W. Chen, L. Lu, F. Jin, and J. Huang, "Space charge behavior evolution with thermal aging of oil-paper insulation," *IEEE Trans. Dielectr. Electr. Insul.*, vol. 22, no. 3, pp. 1381–1388, Jun. 2015.

[22] P. S. Amaro *et al.*, "Investigation of the electrical and chemical processes causing the failure event in a copper sulfide related transformer failure," in *Proc. IEEE Elect. Insul. Conf.*, Jun. 2015, pp. 392–396.

[23] C. Krause, "Power transformer insulation—History, technology and design," *IEEE Trans. Dielectr. Electr. Insul.*, vol. 19, no. 6, pp. 1941–1947, Dec. 2012.

[24] M. K. Pradhan and T. S. Ramu, "On the estimation of elapsed life of oil-immersed power transformers," *IEEE Trans. Power Del.*, vol. 20, no. 3, pp. 1962–1969, Jul. 2005.

[25] S. Y. Matharage, Q. Liu, and Z. D. Wang, "Aging assessment of kraft paper insulation through methanol in oil measurement," *IEEE Trans. Dielectr. Electr. Insul.*, vol. 23, no. 3, pp. 1589–1596, Jun. 2016.

[26] H. H. Han, "Research on transformer aging character and analysis aging mechanism," Ph.D. dissertation, College Electr. Inf. Eng., Changsha Univ. Sci. Technol., Changsha, China, 2007.

[27] J. Ruan *et al.*, "Condition assessment of paper insulation in oil-immersed power transformers based on the iterative inversion of resistivity," *Energies*, vol. 10, no. 4, pp. 509–524, 2017.

[28] A. K. Jonscher, *Dielectric Relaxation in Solids*. London, U.K.: Chelsea Dielectric Press, 1983.

[29] J. Blennow, C. Ekanayake, K. Walczak, B. Garcia, and S. M. Gubanski, "Field experiences with measurements of dielectric response in frequency domain for power transformer diagnostics," *IEEE Trans. Power Del.*, vol. 21, no. 2, pp. 681–688, Apr. 2006.

[30] J. Gao, L. Yang, Y. Wang, C. Qi, J. Hao, and J. Liu, "Quantitative evaluation of ageing condition of oil-paper insulation using frequency domain characteristic extracted from modified cole-cole model," *IEEE Trans. Dielectr. Electr. Insul.*, vol. 22, no. 5, pp. 2694–2702, Oct. 2015.

[31] U. Gafvert, L. Adeen, M. Tapper, P. Ghasemi, and B. Jonsson, "Dielectric spectroscopy in time and frequency domain applied to diagnostics of power transformers," in *Proc. IEEE Int. Conf. Properties Appl. Dielectric Mater.*, Jun. 2000, pp. 825–830.

[32] M. B. Allen and E. L. Isaacson, *Numerical Analysis for Statisticians*. New York, NY, USA: Springer, 1999, pp. 273–290.

JIANGJUN RUAN (M'03) was born in Zhejiang, China, in 1968. He received the B.S. and Ph.D. degrees in electric machine engineering from the Huazhong University of Science and Technology, Wuhan, China, in 1990 and 1995, respectively. He finished his Postdoctoral research at the Wuhan University of Hydraulic and Electric Engineering, Wuhan, in 1998. He is currently a Professor with Wuhan University, Wuhan. His research interests include electromagnetic field numerical simulation, and high-voltage and insulation technology.

YIMING XIE was born in Anhui, China, in 1993. He is currently pursuing the Ph.D. degree in high-voltage and insulation technology with the School of Electrical Engineering and Automation, Wuhan University. His research interests include multi-physical field simulation, condition monitoring of electric device, and high-voltage and insulation technology.

SHUO JIN was born in Henan, China, in 1988. He received the Ph.D. degree from the School of Electrical Engineering and Automation, Wuhan University, in 2018. He is currently a Lecturer with the School of Electrical and Electronic Engineering, Hubei University of Technology. His research interests include multi-physical field simulation, condition monitoring of electric device, and high-voltage and insulation technology.

YU SHI, photograph and biography not available at the time of publication.

YU TIAN, photograph and biography not available at the time of publication.

YONGQING DENG, photograph and biography not available at the time of publication.